Large-Area High-Quality Plasmonic Oligomers Fabricated by Angle-Controlled Colloidal Nanolithography

Jun Zhao,[†] Bettina Frank,[†] Sven Burger,[‡] and Harald Giessen[†,*]

[†]4th Physics Institute and Research Center SCoPE, Pfaffenwaldring 57, University of Stuttgart, 70569 Stuttgart, Germany, and [‡]Zuse Institute Berlin (ZIB), Takustraße 7, 14195 Berlin, Germany

ABSTRACT We introduce angle-controlled colloidal nanolithography as a fast and low-cost fabrication technique for large-area periodic plasmonic oligomers with complex shapes and tunable geometry parameters. We investigate the optical properties and find highly modulated plasmon modes in oligomers with triangular building blocks. Fundamental modes, higher-order modes, as well as Fano resonances due to coupling between bright and dark modes within the same complex structure are present, depending on polarization and structure geometry. Our process is well-suited for mass fabrication of novel large-area plasmonic sensing devices and nanoantennas.

KEYWORDS: large-area high-quality plasmonic oligomers · angle-controlled colloidal nanolithography · higher-order plasmon modes · Fano resonances · plasmonic sensing

Plasmonic oligomers have gained a tremendous amount of attention over the past few years. Self-assembled clusters[1] as well as lithographic structures[2−9] opened up the avenue to plasmonic spectra with well-modulated features. In particular, coupling of bright and dark resonances led to destructive interference of the optical fields and hence to the formation of Fano resonances.[10−16] These resonances have been recognized to exhibit tremendous potential for localized particle plasmon sensing.[17] Applications of refractive index sensing of liquids[18−21] as well as gas sensing[22,23] have been demonstrated.

So far, more widespread applications have been hampered by the necessity to use rather complex and hence expensive electron-beam lithography. Only structures with gaps below 20 nm showed considerably modulated Fano resonances. This fact limits typical fabrication sizes of samples in conventional electron-beam lithography systems to about 100 × 100 μm^2. Samples with larger areas suffer tremendously from inhomogeneities, causing the resonances to shift and hence decreasing their modulation depth.

Here, we introduce an elegant solution to this problem. We utilize colloidal nanolithography[24] to fabricate large-area (10 × 10 mm^2), high-quality plasmonic oligomers with reproducibly small gaps and desired well-defined structural gapless shapes. Our method relies on angle-controlled metal evaporation[25,26] through annealed pinholes between polystyrene spheres. The manufactured oligomers show high-quality fundamental as well as higher-order plasmon resonances with Fano transmittance peaks present.

We analyze the measured and simulated spectra of plasmonic dimers, trimers, and quadrumers and assign the different modes. We find "self-induced" coupling[27,28] between fundamental dipolar modes and higher-order modes within the same structure that leads to Fano resonances. This occurs, in particular, for the case when the plasmonic elements that constitute the oligomer touch each other. For this situation, we examine how structural symmetry breaking allows for tuning the modes and the shapes of the Fano resonances. Finally, we demonstrate that a refractive index sensor with a theoretical figure of merit exceeding 15 can be realized in our structures.

RESULTS AND DISCUSSION

For the fabrication of large-area plasmonic nanostructures, we first prepare a monolayer of hexagonally close-packed polystyrene nanospheres as an evaporation mask, which was described in detail in the paper by Kosiorek *et al.*[29] (preparation details are in the Supporting Information). The evaporation process onto substrates with preannealed polystyrene closed-packed monolayers is performed in a high-vacuum chamber with a pressure of about 10^{-7} Torr using an Edwards E360 evaporation machine. As shown in Figure 1a, the substrate is placed on a face-down sample holder at a distance of d = 25 cm from the metal crucible, tilted by an azimuthal angle θ, which can be controlled by a stepping motor.

* Address correspondence to giessen@physik.uni-stuttgart.de.

Received for review August 18, 2011 and accepted September 29, 2011.

Published online September 29, 2011
10.1021/nn203177s

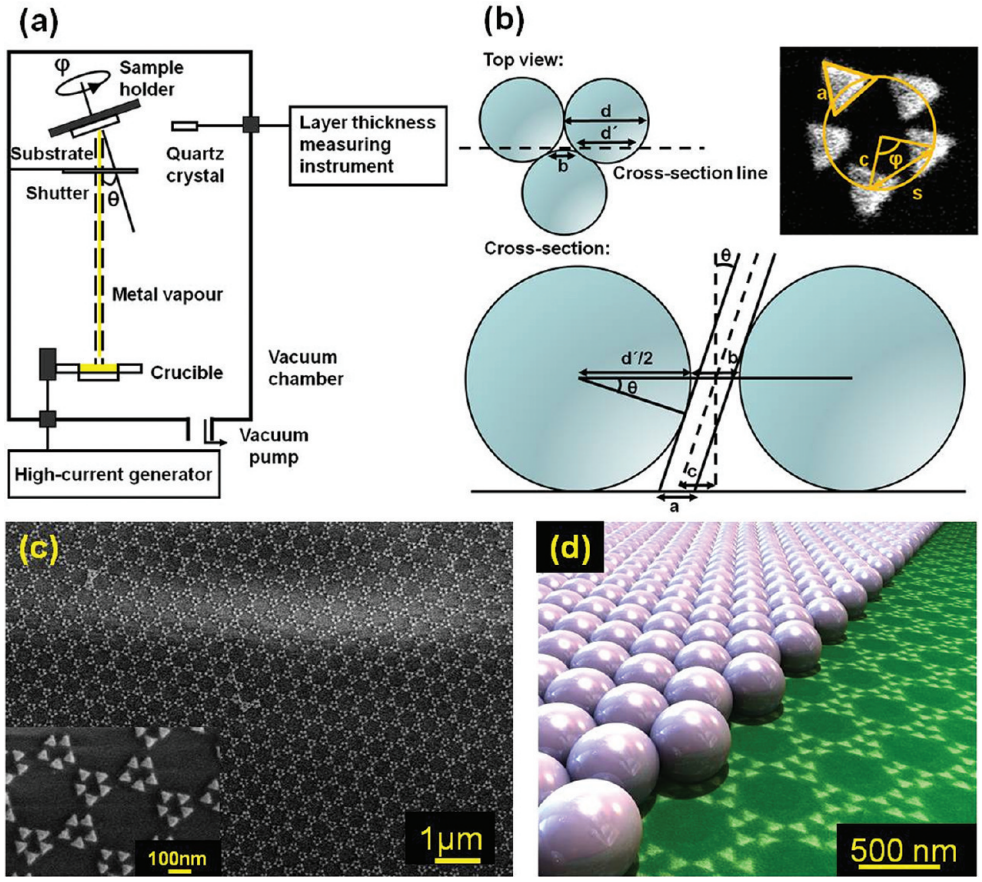

Figure 1. Fabrication of oligomers with triangular building blocks. (a) Schematic diagram of the evaporation setup. (b) Simplified geometrical model for symmetric pentamer fabrication. Top left: top view. Bottom: side view at cross section line as indicated in top view. Top right: geometrical parameters. (c) Scanning electron microscopy (SEM) images of the large area symmetric pentamers. The gap size is as small as 20 nm. The dark-field scattering spectrum is shown in the Supporting Information. (d) Artistic view of our fabrication scheme, using a real SEM image of a symmetric pentamer. The transmittance spectrum of the sample using a large-area optical beam diameter.

Using another stepping motor, the sample holder can be rotated around angle φ in the polar plane. The two stepping motors are software-controlled to accomplish continuous or step-by-step rotation and to set the value of the rotation velocity as well as the evaporation angle. Additionally, we use a programmable shutter between the crucible and the sample. When the shutter is closed, we can change the settings of the two stepping motors, so that some complex structures consisting of different elementary shapes can be prepared. Layer thickness is measured with a quartz microbalance.

During the evaporation process, the metal vapor beam passes through the apertures of the polystyrene monolayer and creates different structures on the glass substrate depending on the evaporation parameters, as shown in Figure 1b. In order to fabricate triangular oligomers, which are arranged on the perimeter of a ring, we set a constant evaporation angle θ. First, a thin layer of chromium is deposited as an adhesive medium, and then gold is evaporated to prepare the first triangle. After that, we rotate the sample by angle φ with the shutter closed and then open the shutter to prepare the next triangle and so on. Because the apertures become smaller while more material is evaporated, in order to fabricate all the triangles in the same size, first only about 10 nm gold is evaporated for each element and then we rotate the sample back to evaporate another 7 nm gold also for each triangle. Less evaporated material and multiple evaporation runs for each element are crucial to achieve the same size of all triangles.

After the evaporation, the nanosphere mask is removed with adhesive tape. The sample is cleaned in *N*-methyl-2-pyrrolidone (NMP) solution in an ultrasonic bath for a few seconds and then flushed with 2-propanol. The inset to Figure 1c shows scanning electron microscope (SEM) images of symmetric pentamers with gaps. Multiple triangular elements can be obtained under each aperture of the nanosphere mask, which is different from the well-known vertically evaporated Fischer patterns.[24] Figure 1c shows the SEM images of our structures over a large area, demonstrating excellent homogeneity and virtually no defects. Figure 1d gives an artistic impression of the fabrication

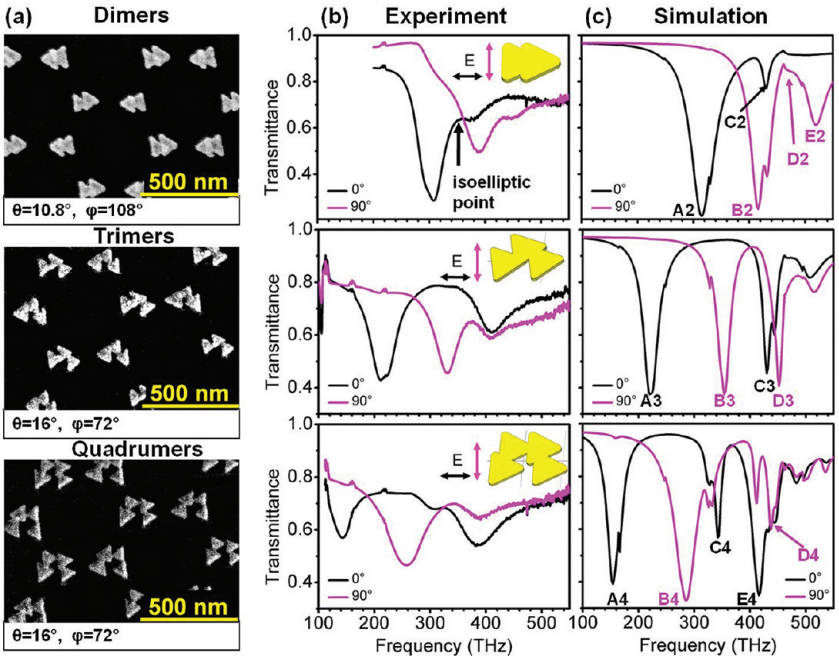

Figure 2. Experimental and simulation results using 500 nm nanospheres and a mask annealing time of 75 s. (a) SEM images of the touching triangular dimers, trimers, and quadrumers with the evaporation and rotation angles θ and φ as depicted in Figure 1a. (b) Experimental transmittance spectra for different polarizations measured with FTIR spectroscopy. (c) Corresponding simulation results (using a finite-element model).

process in the case of symmetric pentamers with fine gaps. Actually, the structures are periodic over the whole 10 × 10 mm^2 glass substrate but contain, as well, some dislocation defects because of cracks of the mask.

Using different fabrication settings, we can control the geometry parameters very precisely. For example, shorter annealing time will result in larger triangles, and smaller angles θ will result in larger triangles and smaller distances between. Therefore, we can tune the dielectric gaps in oligomers on a nanometer distance scale, even until they vanish. In the following, we are going to analyze the fabricated touching oligomers and discuss their optical properties.

In Figure 2, we show the results of our fabricated touching gold oligomers with different numbers of triangular elements, which are arranged as split ring resonators (SRRs). Figure 2a shows the SEM images of touching dimers, trimers, and quadrumers, with the used fabrication parameters. We measured the transmittance spectra (Figure 2b) of the samples at normal incidence with a Fourier transform infrared (FTIR) spectrometer with different electric field polarizations. We define 0° polarization parallel to the interparticle axis between first and last triangle of the oligomers. Figure 2c shows the simulated transmittance spectra obtained with a time-harmonic finite-element solver (FEM code JCMsuite), which agree with our experiments, taking the inhomogeneous broadening of the experimental spectra into account. The inhomogeneous broadening stems from the fact that the apertures between the polystyrene spheres even after annealing do not all have exactly the same diameters. In the SEM images in Figure 2a, we observe two groups of oligomers with differently oriented triangular elements, which are arranged in an approximately mirror symmetric fashion. The reason for this is the opposite orientation of neighboring apertures in our hexagonally close-packed nanosphere monolayer. The difference of the geometry of the two groups of oligomers does not influence the optical spectra very much, except for a slight frequency difference between the resonances of the two different structures in a unit cell, which may lead to a broadening of the resonances in the experimental spectra. In our simulations, we also use a hexagonal unit cell with two groups of triangles with opposite orientations and with feature sizes as in the experiment and as measured by SEM. Bloch periodic boundary conditions are applied which account for the coupling between oligomers within the 2D array. In the measured and in the simulated spectra, we observe at low frequencies fundamental and at higher frequencies higher-order plasmon modes. Pronounced isoelliptical points, where the spectra show the same transmittance value for all polarizations, are observed. These points allow for separation of the fundamental plasmon resonances for the parallel and perpendicular polarization or between neighboring higher-order plasmon modes. In order to study the higher-order modes, we examine the electric field intensity and the current distributions of all resonances, shown in Figure 3.

For dimers, we observe the fundamental dipolar modes A2 and B2 for both polarizations, with an isoelliptical point

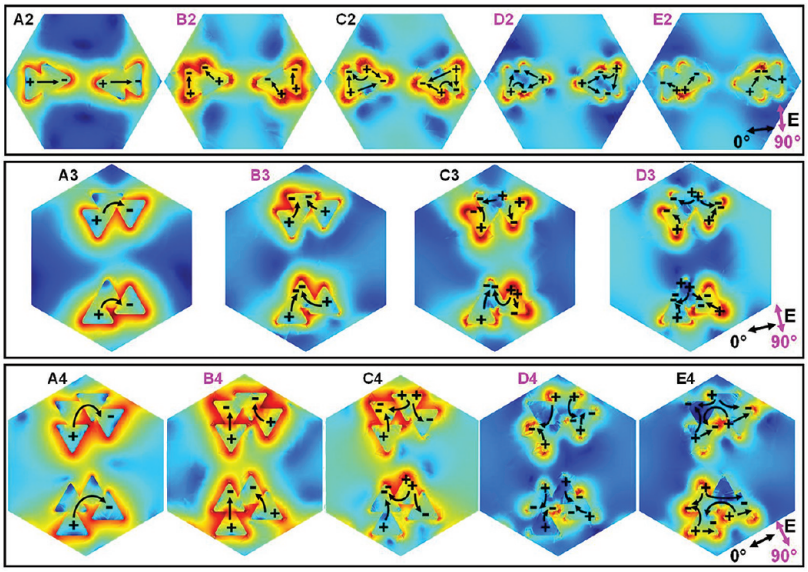

Figure 3. Simulated electric field intensity and current distributions for plasmon modes of touching triangular dimers, trimers, and quadrumers. Black (red) labels refer to 0° (90°) polarization. All of the images show the *XY* cross sections through the simulated field distributions in a unit cell, at $z = 7.5$ nm above the substrate, through the centers of the oligomers. The pseudocolor images display the natural logarithm of the electric field intensity $\log(E^2)$, normalized to the intensity of the incoming plane wave. The color scale spans a range from -4 (blue) to $+8$ (red). The arrows show the current distributions for each mode. In particular, field plots A3 and A4 demonstrate the analogy of the collective plasmonic oligomer modes to the fundamental mode of a split-ring resonator.

separating them. A quadrupolar mode C2 is also observed for 0° polarization as a dip in the transmittance spectrum, which is directly excited by the normally incident light, allowed due to the asymmetric structural geometry with sharp edges. This mode is spectrally located near the dipolar resonance B2 for orthogonal polarization. Additionally, a Fano-type transmittance peak D2 with asymmetric profile appears for 90° polarization, due to the interference of the bright dipolar mode B2 with a dark quadrupolar mode within the same dimer structure. Here, we find the quadrupolar mode in dimers to change from bright to dark when the polarization is rotated from 0 to 90°.

In trimers, due to the SRR-like structure shape, a dipolar mode, namely, the first-order SRR mode (A3), and a second-order (B3), a third-order (C3), and a fourth-order (D3) SRR mode are observable, which are excited either with 0 or 90° polarization and separated by pronounced isoelliptical points. With more triangular elements, the structure shape displays a more SRR-like character. This holds true as well for its optical properties. The D4 mode is usually dark in normal SRR geometry but becomes allowed in our case because of the symmetry breaking due to the sharp triangles.

In quadrumers, all SRR modes A4 to D4 are separated by three isoelliptical points and excited either with 0 or 90° polarization. In the same range as the fourth-order SRR mode D4, a hexapolar nanodisk mode E4 is situated, which is excited by polarization at 0°. Here, we find that the higher-order nanodisk mode and the higher-order SRR mode can be excited simultaneously, due to the complex nonsymmetric structure geometry.

From the experiment and simulation results, we find that higher-order plasmon modes in our touching triangular oligomers can be directly excited by the normally incident light due to the asymmetric structure geometry. The isoelliptical points in the spectra are very useful for identifying the polarization-dependent plasmon modes in our touching oligomers. We can therefore distinguish the bright higher-order modes and the Fano resonance. Additionally, we can observe the higher-order nanodisk modes and the higher-order SRR modes simultaneously in the same structure. In some structures with a lower degree of asymmetry, such as dimers, the higher-order plasmon mode can be also dark for a certain polarization, which couples then with a bright dipolar mode within the same structure and in the same spectral range, resulting in a "self-induced" Fano resonance. A similar situation was found by Nordlander *et al.* in substrate-induced Fano resonances in Ag nanocubes[27] as well as in a single metallic nanodisk with a missing wedge-shaped slice.[28] In some hybridized plasmonic structures with different individual elements, such as nanoparticle aggregates,[5−7,20,30] nonconcentric ring/disk cavities,[19,31,32] or stacked nanostructures,[12] similar effects occurred. However, in these structures, strong coupling between the resonances of individual elements requires small dielectric gaps of just a few nanometers in planar structures or 3D arrangement, which rely on complicated fabrication techniques.

In order to study the modulation depth and hence the strength of higher-order plasmon modes and the

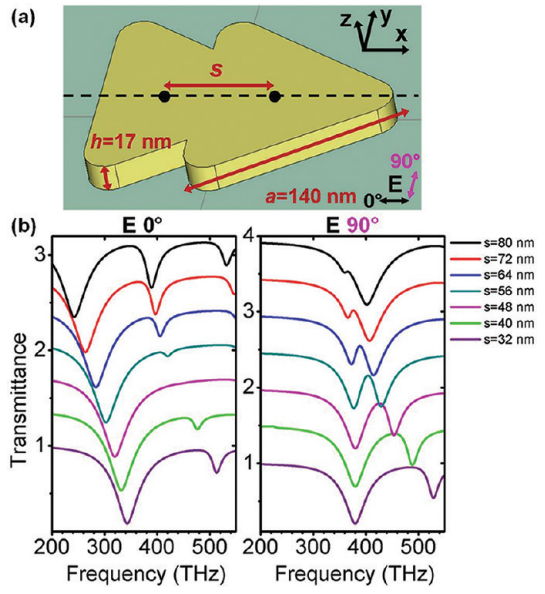

Figure 4. (a) Schematic dimer structure used for simulation with length of the triangle a = 140 nm, thickness h = 17 nm, and distance of two triangles s. The polarization of the used normal incident light 0° is along the x-axis. (b) Simulated transmittance spectra for different distances s with polarization 0° (left) and 90° (right), using CST Microwave Studio.

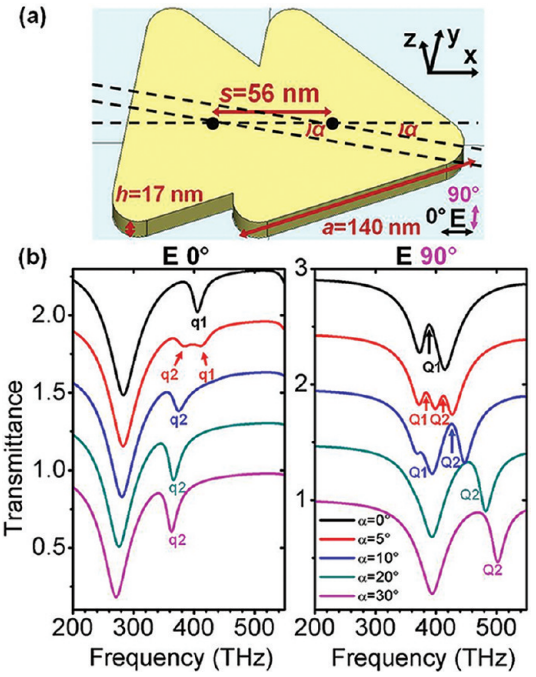

Figure 5. (a) Schematic dimer structure used for simulation with length of the triangle a = 140 nm, thickness h = 17 nm, distance of two triangles s = 56 nm, and rotated angle α around the centers of the triangles. The polarization of the used normal incident light 0° is along the x-axis. (b) Simulated transmittance spectra for different angle α with polarization of 0° (left) and 90° (right), using CST Microwave Studio.

associated Fano resonances that arise due to self-induced coupling effects, we simulate transmittance spectra for dimers with the same triangle length a = 140 nm and thickness h = 17 nm as the fabricated sample shown in Figure 2a at normal incidence, using the frequency domain solver CST Microwave Studio (see Figure 4). In this case, we use a rectangular unit cell and a single group of triangles.

First, we align the two triangles with their interparticle axis along the x-axis and one of their edges pointing in the x-direction. We define s as the distance between the centers of the two triangles. Polarization of 0° is along the x-axis, as depicted in Figure 4a. Figure 4b shows the simulated transmittance spectra for different distances s. For 0° polarization, the fundamental dipolar mode shifts from 250 to 340 THz and the bright quadrupolar mode shifts from 410 to about 510 THz with decreasing s. Additionally, the resonance depth of the quadrupolar mode becomes smaller at first and then larger again. For s = 48 nm, the quadrupolar mode disappears completely in the spectrum, which indicates that the residual dipole moment of the structure is extremely small, and this mode becomes dark. For 90° polarization, we observe a very weak dipole−dipole coupling for large values of distance s (black curve) because of the large residual dipole moment of the quadrupolar mode. With decreasing distance s, the quadrupolar mode becomes dark, resulting in a stronger Fano resonance. Also because of the smaller distance and the same triangle length, the quadrupolar mode shifts blue, whereas the dipolar mode for 90° polarization remains almost at the same position, which results in a more symmetric shape of the Fano resonance. For s smaller than 56 nm, the Fano resonance becomes asymmetric again, as the quadrupolar mode shifts even more toward the blue with decreasing s. The shape of the Fano resonance changes also because the quadrupolar mode becomes bright again with decreasing s and couples directly to the incident light.

Keeping a constant distance s = 56 nm, we now rotate both of the two triangles around their centers and simulate the transmittance spectra for different angle α for both 0 and 90° polarization, as shown in Figure 5. For α = 0°, we observe one bright quadrupolar mode q1 at about 410 THz for 0° polarization. In the case of 90° polarization, we observe coupling of a dark quadrupolar mode Q1 with the bright dipolar mode, leading to a Fano resonance that is visible as a transmittance peak at about 380 THz. In the next step, we lift the degeneracy of the quadrupolar mode by breaking the symmetrical arrangement of the two triangles by rotation of the two triangles 5° around their centers. At 0° polarization, we observe two weak bright quadrupolar resonances q1 and q2 at 410 and 380 THz. For 90° polarization, the removal of the degeneracy leads to a double Fano resonance by interaction of the two dark quadrupolar modes Q1 and Q2 at about 380 and 410 THz with the bright dipole. Afterward, we evaluate the evolution to even more rotation α = 10°.

For 0° polarization, we observe only one bright quadrupolar mode q2. For 90° polarization, the Fano resonance due to the quadrupolar mode Q1 also disappears, while the Fano resonance due to Q2 becomes stronger. With increasing rotation angle α, the two triangles tend to be arranged in a more symmetric fashion with a new symmetry axis. Upon further increased angles α = 20 and 30°, the bright quadrupolar mode q2 for 0° polarization shifts red and the line shape of the Fano resonance Q2 for 90° polarization becomes very similar to that at small distance *s* in Figure 4b because the quadrupolar mode Q2 also becomes bright with larger α and couples directly to the normally incident light.

From these simulations, we infer that the brightness of higher-order plasmon modes in our gapless oligomers depends very strongly on the exact structure geometry. Due to the complex and asymmetric structural shape, most of the characteristic higher-order modes contain some residual dipole moments. Therefore, to determine whether a higher-order mode is dark or bright will depend on its dipole moment being small or large. In order to achieve well-modulated Fano resonances, we should design our touching oligomers with suitable structural asymmetry. The structural geometry should be tuned such that the higher-order mode in this structure is dark, and it should be situated in the same spectral range as the dipolar mode. The number of triangle elements, overlap area, and arrangement of the triangles play the key roles. The self-induced coupling of the bright dipolar and dark higher-order modes in the same structure with well-tuned structural asymmetry can be achieved more easily with our simple fabrication technique.

Due to the localized electric fields and the narrow line shapes, Fano resonances are ideal candidates for localized surface plasmon resonance (LSPR) sensors. In order to test the sensitivity of the Fano resonance in our dimers upon refractive index changes, we analyzed structures with the same symmetric arrangement as in Figure 4a to ensure the darkness of the quadrupolar mode. We used thicker structures with larger size, which are more sensitive to the refractive index of the surrounding medium. Figure 6 shows the simulated transmittance spectra of symmetrically arranged touching dimers with 200 nm triangle length and 40 nm thickness for different surrounding media with thickness h_m = 100 nm. The refractive index is 1.33 (black) and 1.34 (red).

To quantify the sensitivity of the Fano resonance for sensing, we use the figure of merit (FOM) introduced by van Duyne and co-workers[33]

$$\mathrm{FOM} = \frac{\Delta\lambda(\mathrm{nm})}{\Delta n(\mathrm{RIU}) \times \mathrm{fwhm(nm)}}$$

Here $\Delta\lambda/\Delta n$ is the Fano resonance shift per refractive index unit, which is around 530 nm/RIU in our spectra. The full width at half-maximum (fwhm) of

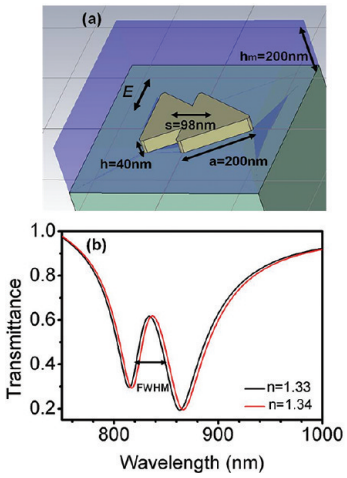

Figure 6. Fano resonances in dimers used for LSPR sensing applications. (a) Schematic diagram of the dimer structures in different dielectric surrounding media. (b) Simulated transmittance spectra for different surrounding media. The refractive index is 1.33 (black) and 1.34 (red). The fwhm of the Fano peak is 30 nm.

the Fano resonance is about 30 nm, and the corresponding FOM of dimers would be around 17. If we use the definition of Nordlander,[30] who considers the distance between the antipeak on the short wavelength side and the peak, in our case, this value would be 21 nm. The corresponding FOM of dimers would then be around 24, which shows that our dimer structure can provide an excellent sensing platform.

CONCLUSIONS

In conclusion, we demonstrated how colloidal lithography in combination with angle-controlled evaporation leads to large-area high-quality plasmonic oligomers. These structures can be fabricated reproducibly with sub-20 nm gaps as well as in a gapless fashion with complex shapes. We analyzed the optical spectra and found fundamental as well as higher-order high-contrast plasmonic resonances. In gapless dimers with appropriate asymmetry, "self-induced" coupling between fundamental dipolar and higher-order plasmon modes within the same structures leads to well-modulated Fano resonances. Refractive index sensors with a figure of merit of more than 15 can be realized in these structures. We believe that our method will open the door toward low-cost, large-area LSPR sensors that rely on the plasmonic analogue of electromagnetically induced transparency. Additionally, our structures could be utilized to combine surface-enhanced Raman scattering (SERS) and surface-enhanced infrared absorption (SEIRA) on a single platform[34] as the fundamental resonances are located in the infrared fingerprint region and can be utilized to enhance vibrational modes of single molecular monolayers.[35] The higher-order modes and the sharp tips of our structures facilitate resonant field enhancement for SERS.[36] The design of suitable nanostructures with a high degree of structural complexity will

enable deep and narrow self-induced Fano resonances. Their combination with simultaneous SEIRA and SERS resonances at multiple wavelengths remains a challenging task for the future.

EXPERIMENTAL DETAILS

The length of the triangular element a depends on the diameter of nanospheres d and the size of apertures b, namely, the annealing time t, as well as on the evaporation angle θ. The aperture size b decreases with longer annealing time. As shown in Figure 1c, the diameter of the nanosphere cross section is $d' = d - b$. The triangle base length is given by

$$a = b(t) + d'\left(1 - \frac{1}{\cos\theta}\right) = d - \frac{1}{\cos\theta}(d - b(t)) \quad (1)$$

The distance s between the centers of two triangles also depends on the polar angle φ as

$$s = 2c \cdot \sin\left(\frac{\varphi}{2}\right) \quad (2)$$

Here, c is the distance of one triangle element from the center of the circle in the inset of Figure 1c. With $c = d/2 \cdot \tan\theta$, we obtain for the distance s between two elements

$$s = d \cdot \tan\theta \cdot \sin\left(\frac{\varphi}{2}\right) \quad (3)$$

With different fabrication settings, we can control the geometry parameters very precisely.

Acknowledgment. We acknowledge N. Strohfeldt for the dark-field scattering measurement, S. Hein for illustrations, and support from DFG (FDR 730, SPP 1391), BMBF (13N9340 and 13N10146), Baden-Württemberg-Stiftung, and German–Israeli Foundation.

Supporting Information Available: Preparation of the polystyrene nanosphere monolayer as an evaporation mask on the glass substrate and the dark-field scattering spectrum of the plasmonic pentamer of Figure 1c. This material is available free of charge *via* the Internet at http://pubs.acs.org.

REFERENCES AND NOTES

1. Fan, J. A.; Wu, C. H.; Bao, K.; Bao, J. M.; Bardhan, R.; Halas, N. J.; Manoharan, V. N.; Nordlander, P.; Shvets, G.; Capasso, F. Self-Assembled Plasmonic Nanoparticle Clusters. *Science* **2010**, *328*, 1135–1138.
2. Halas, N. J.; Lal, S.; Chang, W. S.; Link, S.; Nordlander, P. Plasmons in Strongly Coupled Metallic Nanostructures. *Chem. Rev.* **2011**, *111*, 3913–3961.
3. Brandl, D. W.; Mirin, N. A.; Nordlander, P. Plasmon Modes of Nanosphere Trimers and Quadrumers. *J. Phys. Chem. B* **2006**, *110*, 12302–12310.
4. Alegret, J.; Rindzevicius, T.; Pakizeh, T.; Alaverdyan, Y.; Gunnarsson, L.; Käll, M. Plasmonic Properties of Silver Trimers with Trigonal Symmetry Fabricated by Electron-Beam Lithography. *J. Phys. Chem. C* **2008**, *112*, 14313–14317.
5. Hentschel, M.; Saliba, M.; Vogelgesang, R.; Giessen, H.; Alivisatos, A. P.; Liu, N. Transition from Isolated to Collective Modes in Plasmonic Oligomers. *Nano Lett.* **2010**, *10*, 2721–2726.
6. Hentschel, M.; Dregely, D.; Vogelgesang, R.; Giessen, H.; Liu, N. Plasmonic Oligomers: The Role of Individual Particles in Collective Behavior. *ACS Nano* **2011**, *5*, 2042–2050.
7. Fan, J. A.; Bao, K.; Wu, C. H.; Bao, J. M.; Bardhan, R.; Halas, N. J.; Manoharan, V. N.; Shvets, G.; Nordlander, P.; Capasso, F. Fano-like Interference in Self-Assembled Plasmonic Quadrumer Clusters. *Nano Lett.* **2010**, *10*, 4680–4685.
8. Rahmani, M.; Tahmasebi, T.; Lin, Y.; Lukyanchuk, B.; Liew, T. Y. F.; Hong, M. H. Influence of Plasmon Destructive Interferences on Optical Properties of Gold Planar Quadrumers. *Nanotechnology* **2010**, *22*, 245204.
9. Rahmani, M.; Lukyanchuk, B.; Ng, B.; Tavakkoli, K. G., A.; Liew, T. Y. F.; Hong, M. H. Generation of Pronounced Fano Resonances and Tuning of Subwavelength Spatial Light Distribution in Plasmonic Pentamers. *Opt. Express* **2011**, *19*, 4949–4956.
10. Zhang, S.; Genov, D. A.; Wang, Y.; Liu, M.; Zhang, X. Plasmon-Induced Transparency in Metamaterials. *Phys. Rev. Lett.* **2008**, *101*, 047401-1–4.
11. Papasimakis, N.; Fedotov, V. A.; Zheludev, N. I.; Prosvirnin, S. L. Metamaterial Analog of Electromagnetically Induced Transparency. *Phys. Rev. Lett.* **2008**, *101*, 253903-1–4.
12. Liu, N.; Langguth, L.; Weiss, T.; Kästel, J.; Fleischhauer, M.; Pfau, T.; Giessen, H. Plasmonic Analogue of Electromagnetically Induced Transparency at the Drude Damping Limit. *Nat. Mater.* **2009**, *8*, 758–762.
13. Tassin, P.; Zhang, L.; Koschny, Th.; Economou, E. N.; Soukoulis, C. M. Low-Loss Metamaterials Based on Classical Electromagnetically Induced Transparency. *Phys. Rev. Lett.* **2009**, *102*, 053901-1–4.
14. Chen, J. X.; Wang, P.; Chen, C. C.; Lu, Y. H.; Ming, H.; Zhan, Q. W. Plasmonic EIT-like Switching in Bright-Dark-Bright Plasmon Resonators. *Opt. Express* **2011**, *19*, 5970–5978.
15. Mukherjee, S.; Sobhani, H.; Lassiter, J. B.; Bardhan, R.; Nordlander, P.; Halas, N. J. Fanoshells: Nanoparticles with Built-in Fano Resonances. *Nano Lett.* **2010**, *10*, 2694–2701.
16. Lukyanchuk, B.; Zheludev, N. I.; Maier, S. A.; Halas, N. J.; Nordlander, P.; Giessen, H.; Chong, C. T. The Fano Resonance in Plasmonic Nanostructures and Metamaterials. *Nat. Mater.* **2010**, *9*, 707–715.
17. Stockman, M. I. Nanoscience: Dark-Hot Resonances. *Nature* **2010**, *467*, 541–542.
18. Liu, N.; Weiss, T.; Mesch, M.; Langguth, L.; Eigenthaler, U.; Hirscher, M.; Sönnichsen, C.; Giessen, H. Planar Metamaterial Analogue of Electromagnetically Induced Transparency for Plasmonic Sensing. *Nano Lett.* **2010**, *10*, 1103–1107.
19. Verellen, N.; Sonnefraud, Y.; Sobhani, H.; Hao, F.; Moshchalkov, V. V.; Dorpe, P. V.; Nordlander, P.; Maier, S. A. Fano Resonances in Individual Coherent Plasmonic Nanocavitis. *Nano Lett.* **2009**, *9*, 1663–1667.
20. Lassiter, J. B.; Sobhani, H.; Fan, J. A.; Kundu, J.; Capasso, F.; Nordlander, P.; Halas, N. J. Fano Resonances in Plasmonic Nanoclusters: Geometrical and Chemical Tunability. *Nano Lett.* **2010**, *10*, 3184–3189.
21. Lal, S.; Link, S.; Halas, N. J. Nano-optics from Sensing to Waveguiding. *Nat. Photonics* **2007**, *1*, 641–648.
22. Liu, N.; Tang, M. L.; Hentschel, M.; Giessen, H.; Alivisatos, A. P. Nanoantenna-Enhanced Gas Sensing in a Single Tailored Nanofocus. *Nat. Mater.* **2011**, *10*, 631–636.
23. Tittl, A.; Mai, P.; Taubert, R.; Dregely, D.; Liu, N.; Giessen, H. Palladium-Based Plasmonic Perfect Absorber in the Visible Wavelength Range and Its Application to Hydrogen Sensing. *Nano Lett.* **2011**, DOI: 10.1021/nl202489g.
24. Fischer, U. Ch.; Zingsheim, H. P. Submicroscopic Pattern Replication with Visible Light. *J. Vac. Sci. Technol.* **1981**, *19*, 881–885.
25. Kosiorek, A.; Kandulski, W.; Glaczynska, H.; Giersig, M. Fabrication of Nanoscale Rings, Dots, and Rods by Combining Shadow Nanosphere Lithography and Annealed Polystyrene Nanosphere Masks. *Small* **2005**, *1*, 439–444.
26. Gwinner, M. C.; Koroknay, E.; Fu, L. W.; Patoka, P.; Kandulski, W.; Giersig, M.; Giessen, H. Periodic Large-Area Metallic

Split-Ring Resonator Metamaterial Fabrication Based on Shadow Nanophere Lithography. *Small* **2009**, *5*, 400–406.
27. Zhang, S. P.; Bao, K.; Halas, N. J.; Xu, H. X.; Nordlander, P. Substrate-Induced Fano Resonances of a Plasmonic Nanocube: A Route to Increased-Sensitivity Localized Surface Plasmon Resonance Sensors Revealed. *Nano Lett.* **2011**, *11*, 1657–1663.
28. Fang, Z.; Cai, J.; Yan, Z.; Nordlander, P.; Halas, N. J.; Zhu, X. Removing a Wedge from a Metallic Nanodisk Reveals a Fano Resonance. *Nano Lett.* **2011**, DOI: 10.1021/nl202804y.
29. Kosiorek, A.; Kandulski, W.; Chudzinski, P.; Kempa, K.; Giersig, M. Shadow Nanosphere Lithography: Simulation and Experiment. *Nano Lett.* **2004**, *4*, 1359–1363.
30. Mirin, N. A.; Bao, K.; Nordlander, P. Fano Resonances in Plasmonic Nanoparticle Aggregates. *J. Phys. Chem. A* **2009**, *113*, 4028–4034.
31. Hao, F.; Sonnefraud, Y.; Dorpe, P. V.; Maier, S. A.; Halas, N. J.; Nordlander, P. Symmetry Breaking in Plasmonic Nanocavities: Subradiant LSPR Sensing and a Tunable Fano Resonance. *Nano Lett.* **2008**, *8*, 3983–3988.
32. Hao, F.; Nordlander, P.; Sonnefraud, Y.; Dorpe, P. V.; Maier, S. A. Tunability of Subradiant Dipolar and Fano-Type Plasmon Resonances in Metallic Ring/Disk Cavities: Implications for Nanoscale Optical Sensing. *ACS Nano* **2009**, *3*, 643–652.
33. Sherry, L. J.; Chang, S. H.; Schatz, G. C.; Van Duyne, R. P.; Wiley, B. J.; Xia, Y. Localized Surface Plasmon Resonance Spectroscopy of Single Silver Nanocubes. *Nano Lett.* **2005**, *5*, 2034–2038.
34. Kundu, J.; Le, F.; Nordlander, P.; Halas, N. J. Surface Enhanced Infrared Absorption (SEIRA) Spectroscopy on Nanoshell Aggregate Substrates. *Chem. Phys. Lett.* **2008**, *452*, 115–119.
35. Neubrech, F.; Pucci, A.; Cornelius, T. W.; Karim, S.; Garcia-Etxarri, A.; Aizpurua, J. Resonant Plasmonic and Vibrational Coupling in a Tailored Nanoantenna for Infrared Detection. *Phys. Rev. Lett.* **2008**, *101*, 157403-1−4.
36. Stiles, P. L.; Dieringer, J. A.; Shah, N. C.; Van Duyne, R. P. Surface-Enhanced Raman Spectroscopy. *Annu. Rev. Anal. Chem.* **2008**, *1*, 601–626.